Since January 2020 Elsevier has created a COVID-19 resource centre with free information in English and Mandarin on the novel coronavirus COVID-19. The COVID-19 resource centre is hosted on Elsevier Connect, the company's public news and information website.

Archives of Biochemistry and Biophysics 520 (2012) 74–80

Contents lists available at SciVerse ScienceDirect

Archives of Biochemistry and Biophysics

journal homepage: www.elsevier.com/locate/yabbi

Differential domain structure stability of the severe acute respiratory syndrome coronavirus papain-like protease

Ya-Wen Chou, Shu-Chun Cheng, Hsing-Yi Lai, Chi-Yuan Chou *

Department of Life Sciences and Institute of Genome Sciences, National Yang-Ming University, Taipei 112, Taiwan

ARTICLE INFO

Article history:
Received 12 January 2012
and in revised form 21 February 2012
Available online 3 March 2012

Keywords:
Viral protease
Deubiquitination
Reversible three-state unfolding
Molten globule
Analytical ultracentrifugation

ABSTRACT

Papain-like protease (PLpro) from severe acute respiratory syndrome (SARS) coronavirus is one of the two proteases involved in the proteolytic processing of the virion polyproteins. In addition, PLpro shows significant *in vitro* deubiquitinating and de-ISGylating activities. All these findings demonstrated the multifunctional nature of the PLpro. Here we report the sensitivity of PLpro to denaturant urea. An increase in urea concentration induced a reversible biphasic unfolding of the enzyme. Differently, the unfolding of the catalytic triad region located within the palm and thumb domains followed a monophasic unfolding curve. Further observations suggest that the zinc-binding domain may start to unfold during the first transition. An 80% lost of its enzymatic activity at a urea concentration lower than 1 M showed a close correlation with unfolding of the zinc-binding domain. The enzyme was also characterized in terms of hydrophobicity and size-and-shape distribution. We have demonstrated that PLpro displayed differential domain structure stability and molten globule state in its folding. These studies will not only assist in our understanding of the folding of this viral enzyme, but also that of other deubiquitinating enzymes with a similar scaffold.

Introduction

Severe acute respiratory syndrome (SARS)[1] is a life-threatening atypical pneumonia that emerged in late 2002 and had spread to three continents in 2003 [1]. It is caused by a novel coronavirus (CoV), named SARS-CoV, which infected thousands of people with a 15% fatality rate (World Health Organization). Over the next 2 years, the discovery of two more species of human CoV, NL-63 and HCoV-HKU1, confirmed the high mutation rate of coronaviruses [2,3]. Recent isolation of SARS-CoV like strains from bats further raises the possibility of a reemergence of SARS or a related disease [4,5]. All of these findings result in an urgent need to understand these viruses and their encoded proteins better.

SARS-CoV has two cysteine proteases, a main protease and a papain-like protease (PLpro); these are able to cleave the virion polyproteins (ppla and pp1ab) into 16 nonstructural proteins, including a helicase, a nuclease, a polymerase and others [6]. Both proteases are suitable antiviral targets because they are essential for viral maturation [7,8]. Besides the proteolytic activity that is common to the main protease, PLpro also showed significant deubiquitinating (DUB) and de-ISGylating activities with obscure biological functions [9]. Recently, cellular assays have also suggested that coronaviral PLpro is able to antagonize the induction of type I interferon, which is independent of its protease and DUB activity [10]. All of these studies support the multifunctional nature of the PLpro and suggested that these independent activities may provide multiple targets for antiviral therapies.

Recently, two coronaviral PLpro enzymes have been structurally characterized, namely one from SARS-CoV (PLpro type 2) and the other from transmissible gastroenteritis virus (PLpro type 1) [11,12]. Both of them share a papain-like fold that contains palm, thumb, and fingers domains (Fig. 1A). The active site of PLpro is located within the palm and thumb domains consisting of a catalytic triad of cysteine, histidine, and aspartic acid residues [9]. A four-strand anti-parallel β-sheet makes up the "fingers" domain. Within the fingertips region there are four cysteine residues coordinating to a zinc ion. Mutation of the zinc-coordinating cysteines caused a significant loss of enzymatic activity and this suggests that the zinc-binding ability is essential for its enzymatic function [9].

The structural stability and the folding of coronaviral PLpro have been poorly understood at the present stage. Here we report the reversible unfolding/refolding process of the SARS-CoV PLpro at various urea concentrations. By analyzing the secondary, tertiary and quaternary structural changes of PLpro, a novel folding intermediate was identified, which allow us to delineate the differential stability of the core and zinc-binding domains.

* Corresponding author. Fax: +886 2 28202449.
E-mail address: cychou@ym.edu.tw (C.-Y. Chou).

[1] *Abbreviations used:* AEW, average emission wavelength; ANS, 1-anilino-8-naphthalensulfonicacid; AUC, analytical ultracentrifugation; CD, circular dichroism; CoV, coronavirus; DUB, deubiquitinating; f/f_0, frictional ratio; FG6–*p*NA, FRLKGG-para-nitroanilide; PLpro, papain-like protease; SARS, severe acute respiratory syndrome.

0003-9861/$ - see front matter © 2012 Elsevier Inc. All rights reserved.
doi:10.1016/j.abb.2012.02.015

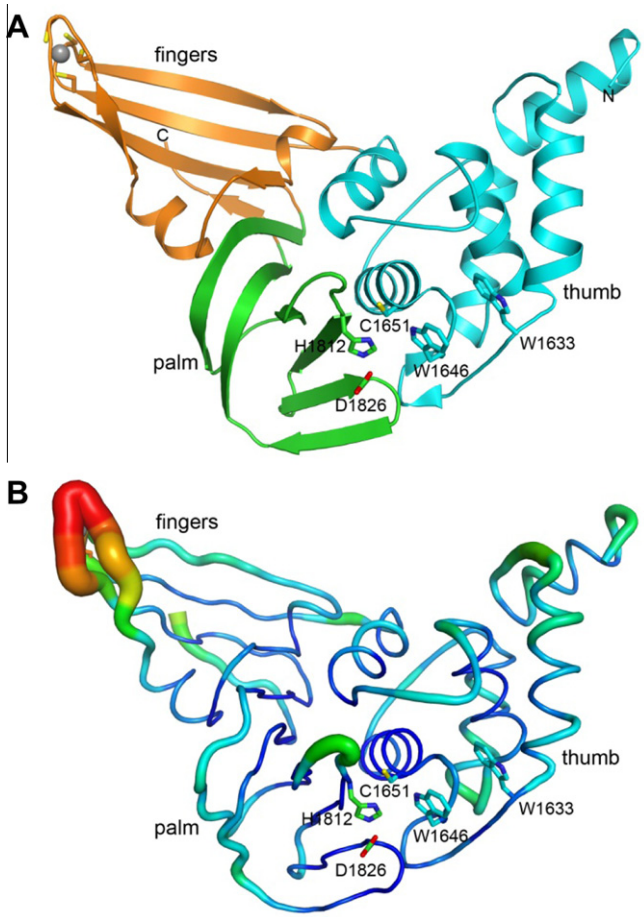

Fig. 1. Structure of the SARS-CoV PLpro 1600–1858 fragments. (A) The original structure was 2FE8 (pdb) [11], the ubiquitin-like domain of which was removed. The thumb, palm, and fingers domains are colored by cyan, green, and orange, respectively. The catalytic triad, the two tryptophans, and the four zinc coordinated cysteines are shown as sticks. The gray sphere is zinc. (B) The structural flexibility of the enzyme is shown as a variable worm of the polypeptide chain. The temperature factor from low to high is colored by rainbow (blue to red). The more flexible regions are shown as a thicker worm. The plots are generated by Pymol [34]. (For interpretation of the references to color in this figure legend, the reader is referred to the web version of this article.)

Materials and methods

Plasmid

The PLpro-(1541–1858) and PLpro-(1600–1858) DNA fragments were amplified by PCR. The forward primer for the 1541–1858 fragment was 5′-aattaaacatatggaggttaagactataaaagtg and for the 1600–1858 fragment was 5′-aattaaacatatgagtgatgacacactacg; the reverse primer in both cases was 5′-acgctcgagcgacacaggcttgatggttg. The PCR fragments were then digested with *Nde*I–*Xho*I and each ligated independently into *Nde*I–*Xho*I digested pET-22b(+) vector (5.2 kb). The nucleotide sequences were confirmed by autosequencing analysis.

Expression and purification of the PLpro proteins

The protein induction and purification procedures have been described previously [7]. Typical yields of the PLpro proteins were 10–12 mg after purification from 1 L of *Escherichia coli* in culture medium. The purity was estimated by SDS–PAGE to be >95% and the molecular mass of PLpro-(1541–1858) and PLpro-(1600–1858) were estimated to be 35 and 30 kDa, respectively. The purified proteins were buffer-changed to 50 mM sodium phosphate buffer (pH 7.4) using Amicon Ultra-4 10-kDa centrifugal filter (Millipore).

Enzyme kinetic assay

The enzymatic activity of PLpro was measured by a colorimetry-based peptide cleavage assay involving the 6-mer peptide substrate, FRLKGG–para-nitroanilide (FG6–*p*NA) (purity 95% by HPLC; GL Biochem Ltd., Shanghai, China). This substrate is cleaved at the Gly–*p*NA bond to release free *p*NA, which turns the color of the solution to yellow. The increase in absorbance at 405 nm was continuously monitored using a Jasco V-550 UV/Vis spectrophotometer (Tokyo, Japan). The amount of *p*NA released by proteolysis can be calculated using a standard curve generated with analytical grade *p*NA and the results are consistent with those reported in the literature ($A_{405\ nm}$ = 9.8 at 1 mM) [13]. The protease activity assay was performed in 50 mM phosphate (pH 7.4) at 30 °C. The substrate stock solution was made up at 4 mM and the working concentrations were from 0.5 to 3.5 mM. The concentration of the enzyme used was 1 μM. The steady state enzyme kinetic parameters were obtained by fitting the initial velocity (v_0) data to the Michaelis–Menten Eq. (1).

$$v_0 = \frac{k_{cat}[E][S]}{K_m + [S]} \quad (1)$$

where k_{cat} is the catalytic constant, [*E*] is the enzyme concentration, [*S*] is the substrate concentration and K_m is the Michaelis constant of the substrate. The program SigmaPlot (Systat Software, Inc., Richmond, CA) was used for the data analysis.

Reversible unfolding/refolding of the enzyme in urea

SARS-CoV PLpro-(1600–1858) was unfolded at various concentrations of urea in 50 mM phosphate (pH 7.4), without or with 50 or 100 mM EDTA, and 25 °C for 1 h to reach equilibrium. In the present study, the unfolding of the enzyme was monitored by circular dichroism (CD), fluorescence, analytical ultracentrifugation (AUC), and enzyme activity loss.

Activity assay in urea

The proteolytic activities of PLpro at various urea concentrations were monitored using 2 mM of FG6–*p*NA and 3.3 μM of the enzyme. For the DUB assay, 0.5 μM of ubiquitin-AFC (Boston Biochem, Cambridge, MA) and 0.4 μM of PLpro were used [7]. The enzymatic activities at various urea concentrations were determined by monitoring the enhanced fluorescence emission upon substrate cleavage at the excitation and emission wavelengths of 350 and 485 nm, respectively, using a Perkin–Elmer LS50B luminescence spectrometer (USA) at 30 °C.

Circular dichroism spectroscopy

The CD spectra of the enzyme was measured at 25 °C in 50 mM phosphate (pH 7.4) with various urea concentrations using a JASCO J-810 spectropolarimeter (Tokyo, Japan), which gave measurements from 230 to 215 nm. Urea was included in the buffer that was used for baseline scanning. The protein concentration was 15 μM and the width of the cuvette was 1 mm.

Spectrofluorimetric analysis

The fluorescence spectra of the enzyme at 0.6 or 1 μM were monitored in a Perkin–Elmer LS50B luminescence spectrometer

at 25 °C. The excitation wavelength was set at 280 or 295 nm (for tryptophan emission), and the fluorescence emission spectrum was scanned from 300 to 400 nm. Changes in the maximal peak, intensity, and average emission wavelength (AEW) were used to monitor the unfolding process [14].

ANS spectrofluorimetric analysis

The fluorescent dye, 1-anilino-8-naphthalensulfonic acid (ANS), was used as the hydrophobic exposure detecting probe [14–16]. Briefly, a fixed concentration of ANS (200 μM) was mixed with the protein (3 μM) at various urea concentrations. The excitation wavelength was set at 395 nm and the emission spectrum was monitored from 410 to 600 nm. The excitation and emission slits were both set at 4 nm.

Analytical ultracentrifugation analysis

The AUC experiments were performed on a XL-A analytical ultracentrifuge (Beckman, Fullerton, CA) using an An-50 Ti rotor [15,17–20]. The sedimentation velocity experiments were performed using a double-sector *epon* charcoal-filled centerpiece at 20 °C with a rotor speed of 42,000 rpm. The sample (330 μl) and reference (370 μl) solutions were loaded into the centerpiece. The absorbance at 280 nm was monitored in a continuous mode with a time interval of 400 s and a step size of 0.003 cm. The protein concentrations of 13 μM in 50 mM phosphate buffer at various concentrations of urea. Multiple scans at different time intervals were then fitted to a continuous $c(s, f/f_0)$ distribution model using the SEDFIT program [14,21–23]. The partial specific volume of the PLpro, the solvent density, and the viscosity were calculated by SEDNTERP (http://www.jphilo.mailway.com/download.htm) (cited June 20, 2011). All size-and-shape distributions were analyzed at a confidence level of $p = 0.95$ by maximal entropy regularization and a resolution N of 200 with sedimentation coefficients between 0 and 20 S. The frictional ratio (f/f_0) is set from 1 to 5 at a resolution of 10.

Unfolding data analysis

The unfolding/refolding of PLpro is a reversible process (Fig. 2) and therefore the unfolding data were analyzed using the following thermodynamic models by global fitting of the CD and fluorescent measurements to either Eq. (2) or Eq. (3):A two-state unfolding model is described by Eq. (2) [24]:

$$y_{obs} = \frac{y_N + y_U \cdot e^{-\left(\frac{\Delta G_{(H_2O)N\to U} - m_{N\to U}[Urea]}{RT}\right)}}{1 + e^{-\left(\frac{\Delta G_{(H_2O)N\to U} - m_{N\to U}[Urea]}{RT}\right)}} \quad (2)$$

A three-state unfolding model is described by Eq. (3) [25]:

$$y_{obs} = \frac{y_N + y_I \cdot e^{-\left(\frac{\Delta G_{(H_2O)N\to I} - m_{N\to I}[Urea]}{RT}\right)} + y_U \cdot e^{-\left(\frac{\Delta G_{(H_2O)N\to I} - m_{N\to I}[Urea]}{RT}\right)} \cdot e^{-\left(\frac{\Delta G_{(H_2O)I\to U} - m_{I\to U}[Urea]}{RT}\right)}}{1 + e^{-\left(\frac{\Delta G_{(H_2O)N\to U} - m_{N\to U}[Urea]}{RT}\right)} + e^{-\left(\frac{\Delta G_{(H_2O)N\to I} - m_{N\to I}[Urea]}{RT}\right)} \cdot e^{-\left(\frac{\Delta G_{(H_2O)I\to U} - m_{I\to U}[Urea]}{RT}\right)}} \quad (3)$$

where y_{obs} is the observed biophysical signal and y_N, y_I, and y_U are the calculated signals of the native, intermediate, and unfolded states, respectively. [Urea] is the urea concentration, and ΔG_{N-U}, ΔG_{N-I}, and ΔG_{I-U} are the free energy changes for the $N \leftrightarrow U$, $N \leftrightarrow I$, and $I \leftrightarrow U$ processes, respectively. Finally, m_{N-U}, m_{N-I}, and m_{I-U} are the sensitivities of the respective unfolding process to denaturant concentration.

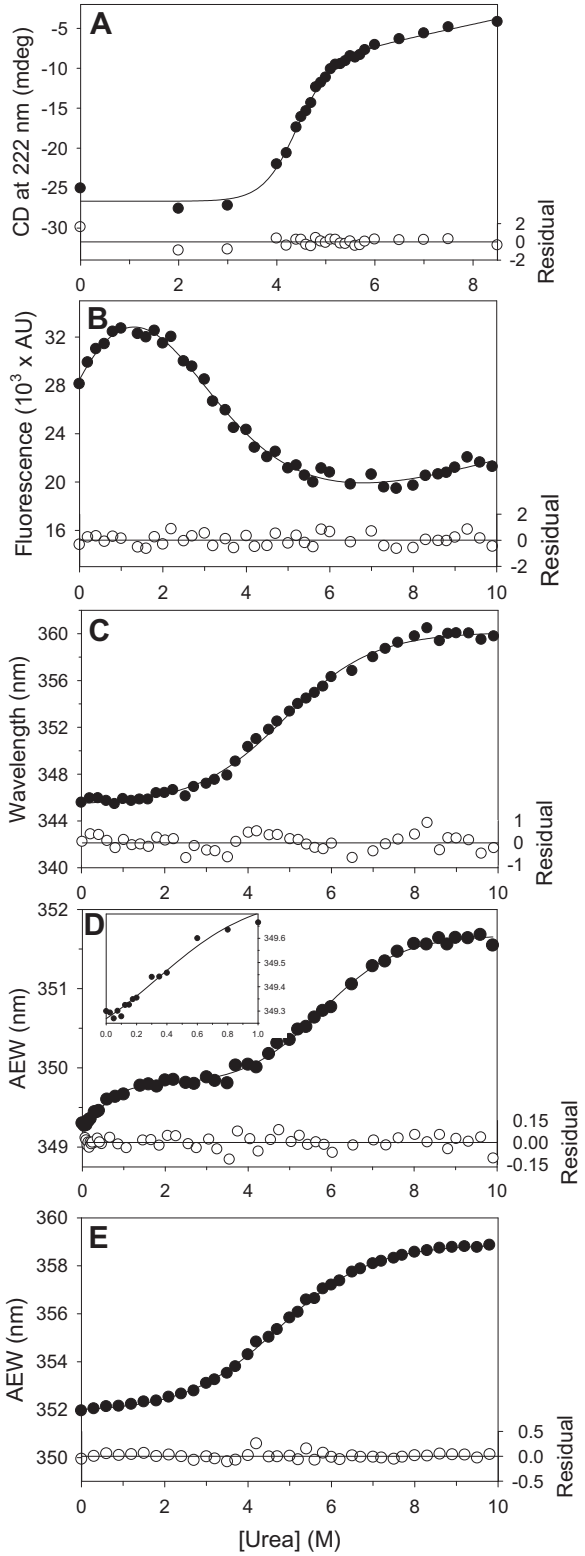

Fig. 2. Unfolding curves of the SARS-CoV PLpro in various concentrations of urea. The enzyme at 15 μM (A), 0.6 μM (B–D), and 1 μM (E) in 50 mM phosphate buffer (pH 7.4) was mixed with various concentrations of urea. After 1-h incubation at 25 °C, the CD spectrum (A) and the fluorescence (B–E) were measured. (A) The ellipticity changes at 222 nm. (B) Integrated fluorescence area from 300 to 400 nm excited at 280 nm. (C) Fluorescence emission wavelength shift. (D) Average fluorescence emission wavelength (AEW) excited at 280 nm. The inset shows the results from 0 to 1 M urea. (E) AEW excited at 295 nm. The closed circles are the experimental data and the lines are the best fit results, according to the two-state unfolding model (Eq. (2)) or the three-state unfolding model (Eq. (3)), respectively. The fitting residuals are shown under each panel (open circles).

Results and discussion

The SARS-CoV PLpro-(1600–1858) fragment is capable of catalysis

The crystal structure of SARS-CoV PLpro suggested a catalytic domain between the residues 1542–1858 of the SARS-CoV polyprotein [11]. The first 62 residues form an independent Ub like domain, whose significance in the catalytic activity is not well understood. Initially we analyzed the catalytic activities of PLpro with and without the Ub like domain. Their kinetic parameters are summarized in Table 1. The k_{cat} of PLpro-(1600–1858) is slightly higher than that of PLpro-(1541–1858), while the K_m of PLpro-(1541–1858) is about 2.5-fold lower and k_{cat}/K_m is twofold higher. The results indicated that their catalytic abilities are quite comparable. The results suggested that the PLpro-(1600–1858) fragment, which contains the palm, thumb, and zinc-finger domain (Fig. 1A), is sufficient and active in terms of catalysis. Next, the unfolding of PLpro-(1600–1858) (shortened to "PLpro" below) was studied to delineate the functional roles and stability of its three constituting domains.

Reversible unfolding of SARS-CoV PLpro in urea

By CD measurement, the thermal denaturation of SARS-CoV PLpro showed a monophasic unfolding process which is irreversible because of serious precipitation after 70 °C is reached (data not shown). As a result of this preliminary finding, chemical denaturation was chosen to analyze PLpro unfolding. Under the excitation at 280 nm, the fluorescence emission spectrum of the native enzyme shows a maximum at 346 nm (Supplemental Fig. 1, solid curve). In the presence of 7 M urea, the enzyme was completely unfolded after 1 h and the maximum emission had shifted to 357 nm (Supplemental Fig. 1, short dashed curve). After 50-fold dilution of the urea and incubation for 10 min, refolding of the enzyme was induced to give a yield of 88% as judged by the fluorescence spectrum recovery (Supplemental Fig. 1, dotted curve). By DUB assay, the refolded enzyme still showed 54% catalytic activities. It indicates that the unfolding of PLpro by urea is a reversible process and suitable for the conformational stability studies of the enzyme.

Unfolding curves of SARS-CoV PLpro in different concentrations of urea

The unfolding of the secondary structure of SARS-CoV PLpro in various concentrations of urea was measured by CD at 222 nm (Fig. 2A). There was a monophasic unfolding process which indicated that PLpro started to unfold beyond 3 M urea, reaching an unfolding intermediate with $[Urea]_{0.5,N-U}$ at 4.4 M (Table 2). The changes of CD signal at 216 nm, which can be used to judge the β-strand content also showed the same unfolding process (Supplemental Fig. 2).

The unfolding of the tertiary structure of the enzyme was measured by fluorescence spectrometry. When the integrated fluorescence area was calculated, a monophasic unfolding process was obtained (Fig. 2B). There is a strong denaturant dependent pretransition slope, which might indicate exposure of hydrophobic areas [14,26]. Similarly, the fluorescence emission peak showed a monophasic red shifting from 345 to 360 nm (Fig. 2C). By fitting these results to the two-state unfolding model, the overall tertiary structural unfolding of PLpro was found to have reached an unfolding intermediate with a $[Urea]_{0.5,N-U}$ at 4.8 M, which is very close to that of secondary structural unfolding (Table 2). Further interesting results are shown in Fig. 2D, where there is an obvious biphasic red shift of the AEW from 349 to 352 nm upon increasing the urea. The data fit to the three-state unfolding model very well, which suggest that the folded enzyme started to unfold at a very few urea and reached the first unfolding intermediate with a $[Urea]_{0.5,N-I}$ at 0.35 M. The second unfolding phase started at ~3.5 M urea with a $[Urea]_{0.5,I-U}$ at 5.8 M, corresponding to free energy changes of 0.77 and 3.68 kcal/mol for the N ↔ I and I ↔ U processes, respectively.

The intermediate state suggests the existence of a zinc-binding domain unfolded structure

We try to characterize the intermediate state between 1 and 3.5 M urea further. Unlike 18 tyrosine residues randomly distributed in PLpro, there are only two tryptophan residues (W1633 and W1646) and both of them are near the active site (Fig. 1). The tryptophan fluorescence thus is an excellent tool to probe the unfolding of the thumb and palm domain (Fig. 2E). A monophasic unfolding process with a $[Urea]_{0.5,N-U}$ at 4.7 M similar to those from CD and fluorescence peak shifting indicated that the unfolding of the catalytic core occurs during the second transition (Table 2). To find out the possible region that may unfold in the first transition, the temperature factors of the residues from the PLpro structure were analyzed (Fig. 1B). The higher temperature factor of the zinc-binding domain than other regions suggests that the first transition may be due to its unfolding.

To identify the influence of zinc-binding on the PLpro structure, we tried to measure the denaturation of PLpro in the presence of EDTA, which is used to remove the endogenous zinc ion from the PLpro. Our results indicated that, the secondary structural unfolding of PLpro in various concentrations of urea and 50 mM EDTA was similar to that without chelates (Supplemental Fig. 3A). There was a monophasic unfolding process reaching an unfolding intermediate with $[Urea]_{0.5,N-U}$ at 4.4 M (Table 2). On the other hand, the fluorescent results suggested that the tertiary structural unfolding of PLpro in various concentrations of urea and 100 mM EDTA was a two-state process (Supplemental Fig. 3B–E). The overall tertiary structural unfolding of PLpro in the presence of EDTA was found to have reached an unfolding intermediate with a $[Urea]_{0.5,N-U}$ at 3.7–3.9 M (Table 2). Comparing to those of PLpro with endogenous zinc, $[Urea]_{0.5,N-U}$ of PLpro without metal ion show a 0.8–1.1 M decrease. The differences provide the direct evidence that zinc-binding can enhance the structural stability of the enzyme.

Exposure of the hydrophobic region of SARS-CoV PLpro during urea denaturation

ANS was used to examine the exposure of the hydrophobic region of PLpro during urea denaturation (Supplemental Fig. 4). There was a pronounced enhancement of ANS fluorescence at 3–4 M urea, which corresponds to the urea concentration at which the tertiary but not secondary structure of palm and thumb domain starts to unfold (Fig. 2D and E). This may represent a molten globule state (see below). In this context, during the first unfolding transition and the first half of the intermediate state (0–2 M urea), there is no significant hydrophobic exposure.

Table 1
Enzyme kinetic parameters of different PLpro fragments.

PLpro	K_m[a] (mM)	k_{cat}[a] (s^{-1})	k_{cat}/K_m[a] ($mM^{-1}\ s^{-1}$)
1541–1858	0.73 ± 0.08	0.79 ± 0.04	1.08 ± 0.13
1600–1858	1.84 ± 0.24	0.96 ± 0.06	0.52 ± 0.08

[a] The steady-state kinetic parameters of PLpro were determined by the Michaelis–Menten equation (Eq. (1)). After best fitting, R_{sqr} of the two fragments were 0.997 and 0.994, respectively. The assays were repeated several times and gained similar results.

Table 2
Stability parameters of SARS-CoV PLpro during the urea unfolding process.

Physical probes[a]	EDTA[c]	ΔG_{N-U} (kcal mol^{-1})	m_{N-U} (kcal mol^{-1} M^{-1})	$[Urea]_{0.5,N-U}$ (M)			
CD (222 nm)	+	14.50 ± 3.16	3.27 ± 0.72	4.4 ± 1.3			
	–	7.62 ± 0.66	1.74 ± 0.15	4.4 ± 0.5			
Fluorescence (intensity)	+	1.84 ± 0.60	0.58 ± 0.13	3.2 ± 1.3			
	–	3.45 ± 0.40	1.03 ± 0.11	3.3 ± 0.5			
λ_{max}	+	2.88 ± 0.18	0.79 ± 0.05	3.7 ± 0.3			
	–	2.76 ± 0.13	0.57 ± 0.03	4.8 ± 0.3			
AEW (Ex 295 nm)	+	2.34 ± 0.16	0.59 ± 0.04	3.9 ± 0.4			
	–	2.60 ± 0.05	0.55 ± 0.01	4.7 ± 0.1			
AEW (Ex 280 nm)	+	2.93 ± 0.37	0.79 ± 0.12	3.7 ± 0.8			
Physical probes[b]	EDTA[c]	ΔG_{N-I} (kcal mol^{-1})	m_{N-I} (kcal mol^{-1} M^{-1})	$[Urea]_{0.5,N-I}$ (M)	ΔG_{I-U} (kcal mol^{-1})	m_{I-U} (kcal mol^{-1} M^{-1})	$[Urea]_{0.5,I-U}$ (M)
AEW (Ex 280 nm)	–	0.77 ± 0.52	2.22 ± 0.66	0.35 ± 0.25	3.68 ± 0.19	0.64 ± 0.03	5.8 ± 0.4

[a] The unfolding data were fitted to a two-state unfolding model according to Eq. (2). The R_{sqr} were from 0.970 to 0.999, respectively.
[b] The unfolding data were fitted to the three-state unfolding model, according to Eq. (3). The R_{sqr} was 0.997.
[c] The concentration of EDTA was 50 mM in CD experiments and 100 mM in fluorescent measurements.

Size-and-shape changes of SARS-CoV PLpro in the presence of urea

Next, the size distribution of PLpro was analyzed by AUC. Supplemental Fig. 5A shows a typical sedimentation velocity profile for the enzyme in phosphate buffer (pH 7.4). By continuous $c(s, f/f_0)$ distribution analysis, the native PLpro showed a single species of $s = 2.9$, which corresponds to a monomer (Supplemental Fig. 5B). The size distributions of the enzyme at various urea concentrations were then analyzed (Supplemental Fig. 5C–H). As the urea increase, the sedimentation coefficient of the major species showed a clearly decrease from 2.9 to 1.0 (Fig. 3, triangles). Multi-peaks distribution at 1.1 M urea (Supplemental Fig. 5D) and an asymmetric peak shape at 2.0 M urea (Supplemental Fig. 5E) suggest a dynamically size-and-shape change during the intermediate state [18,23]. Furthermore, the shape distributions of the PLpro's major species at various urea concentrations were analyzed in terms of their f/f_0 distribution (Fig. 3, color contour). The f/f_0 of the native PLpro was between 1 and 3, while that of the most concentrated region (shown by red) was below 1.5. Before the second unfolding phase (1–3.5 M urea), the broad f/f_0 distribution of the major species suggested a tendency to elongate among the unfolding process, which is similar to that of the SARS-CoV main protease in guanidinium chloride [14]. Based on previous studies, the partial unfolding intermediate may represent a molten globule state with exposure of the interior hydrophobic area, which will allow a pronounced binding of ANS, a broad f/f_0, and higher propensity to aggregate [14,27]. Indeed, at lower protein concentrations of PLpro (<6.5 μM), there is significant aggregation at 3.5 M urea. The ANS binding activity of the urea-unfolded enzyme also showed a significant hydrophobic region exposure between 3 and 4 M urea (Supplemental Fig. 4). All of these results support the presence of a major intermediate form detectable at urea concentrations between 1 and 3.5 M that may only represent a molten globule state after 2.5 M urea. Thus, during the first unfold state and the first half of the intermediate state, the possibility remains that differential domain stability occurs. Above 4.7 M urea, the PLpro showed a sedimentation coefficient of 1.0–1.5 and the f/f_0 of the most concentrated region was close to 2 (Fig. 3). The small sedimentation coefficient and large f/f_0 suggested a totally unfolded protein structure [14,16].

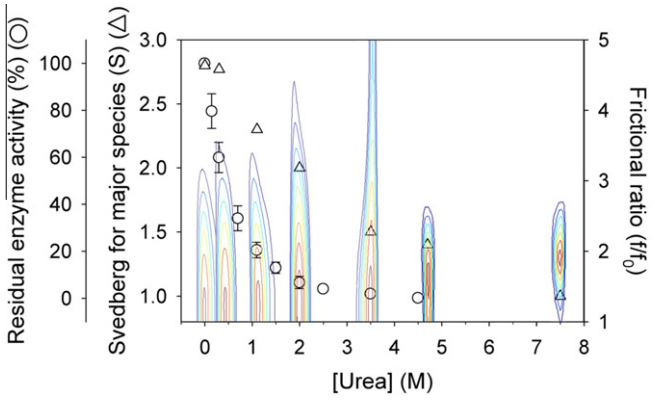

Fig. 3. Urea-induced size-and-shape changes and unfolding of the SARS-CoV PLpro. Open circles show the remaining proteolytic activity and open triangles show the sedimentation coefficients for the major species. Unfolding of the enzyme is demonstrated by the contour of continuous sedimentation coefficient and frictional ratio (f/f_0) with the most concentrated region shown in red. The x axis of these contours has no physical meaning. (For interpretation of the references to color in this figure legend, the reader is referred to the web version of this article.)

The significant enzyme activity loss before the intermediate state

Enzymatic activity change during urea unfolding was examined. The results shown in Fig. 3 (circles) are those for residual enzyme activity by the peptide cleavage assay and similar results were obtained by the DUB assays (data not shown). Interestingly, the enzyme activity began to decrease at very low urea concentrations (50% left at 0.5 M urea). By the time that 1.1 M urea has been reached, there was only 20% of the original activity left. Besides, to identify the influence of endogenous zinc ion, the enzyme activity was also examined in various concentrations of EDTA. The activity was 90% in 10 mM, 50% in 50 mM, while the lowest one was 38% left in 100 mM EDTA. These results support the hypothesis that the first transition, which is caused by the unfolding of zinc-binding site, already has a great deal of influence on activity even when the active core domain still remains folded. According to the modeled structure by Ratia et al. [11], the finger region of PLpro may be used to cradle the body of ubiquitin. It suggested that the zinc-binding site may stabilize the finger region and its unfolding can be detrimental to substrate binding and cause the loss of the activity. Taken together, our studies provide evidence that the structural integrity of zinc-binding site is essential for the enzyme activity [9,11].

Conclusion

In summary, our studies have revealed the reversible unfolding/refolding process of the PLpro in the presence of urea (Fig. 4). The zinc-binding domain of the enzyme may start to unfold at urea concentration below 0.35 M and reaches a first plateau at 1–3.5 M. At this stage, the palm and thumb core domains remain well folded but totally inactive. Remove of zinc ion from the enzyme

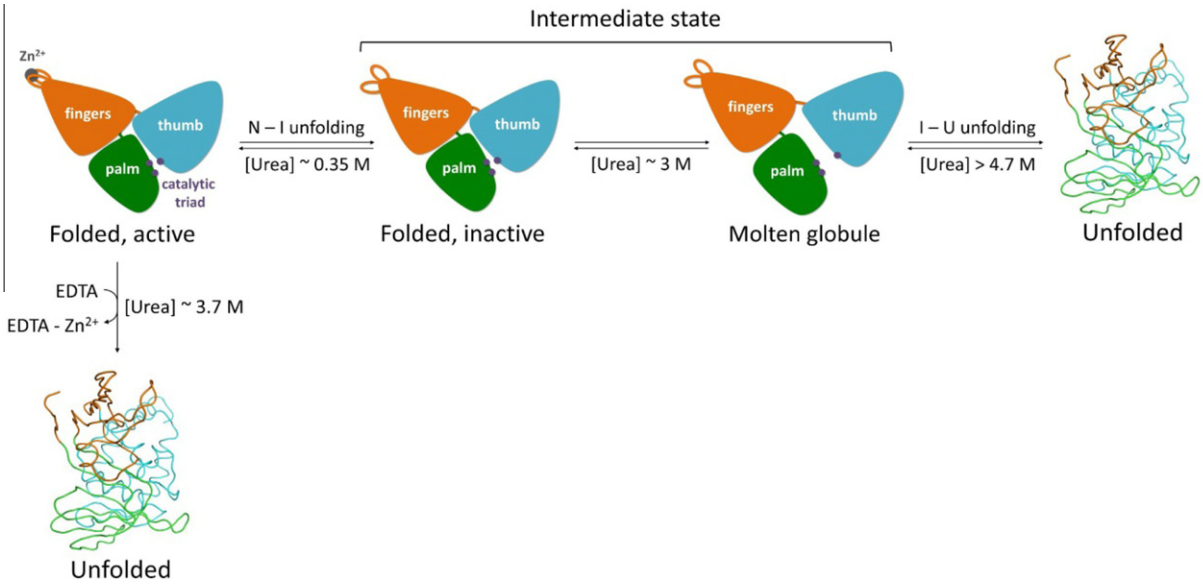

Fig. 4. A schematic model for the unfolding of SARS-CoV PLpro in urea. The PLpro shows a three-state unfolding in the presence of urea. The first half of the intermediate state is suggested as a folded but inactive form, while the late intermediate state should be a molten globule. In the intermediate state, the zinc ion is lost due to the zinc binding motif unfolding. Without zinc ion, PLpro will follow a two-state unfolding and is more unstable.

will cause the tertiary structure more unstable and a two-state unfolding. This supports the hypothesis that the zinc-binding domain can stabilize the structure and is essential for the catalysis [9]. As the urea concentration is increased above 3.5 M, the unfolding of the palm and thumb domain then starts and this involves significant hydrophobic exposure and is completed at 7.5 M urea. This schematic representation only includes the major enzyme species that occur during the folding process. Specifically, PLpro displays a differential stability in terms of the protein's domain structures and a molten globule state is present at the beginning of palm and thumb domain unfolding. Differential domain stability can also be seen in SARS-CoV main protease, while other proteins, such as human alkaline phosphatase, human apolipoprotein E, and malic enzyme have been shown to undergo a significant molten globule transition state during the unfolding process [14,16,28,29]. Our unfolding studies on SARS-CoV PLpro will not only assist in our understanding of the structure folding of this important viral enzyme, but also that of other DUB enzymes with a similar scaffold but low sequence identities, such as HAUSP, USP-2, USP-14 etc. [30–33].

Acknowledgments

We thank G.G. Chang for helpful discussions. This research was supported by grants from National Science Council, Taiwan (98-2320-B-010-026-MY3) and National Health Research Institute, Taiwan (NHRI-EX101-9947SI) to C.-Y.C.

Appendix A. Supplementary data

Supplementary data associated with this article can be found, in the online version, at doi:10.1016/j.abb.2012.02.015.

References

[1] P.A. Rota, M.S. Oberste, S.S. Monroe, W.A. Nix, R. Campagnoli, J.P. Icenogle, S. Penaranda, B. Bankamp, K. Maher, M.H. Chen, S. Tong, A. Tamin, L. Lowe, M. Frace, J.L. DeRisi, Q. Chen, D. Wang, D.D. Erdman, T.C. Peret, C. Burns, T.G. Ksiazek, P.E. Rollin, A. Sanchez, S. Liffick, B. Holloway, J. Limor, K. McCaustland, M. Olsen-Rasmussen, R. Fouchier, S. Gunther, A.D. Osterhaus, C. Drosten, M.A. Pallansch, L.J. Anderson, W.J. Bellini, Science 300 (2003) 1394–1399.
[2] L. van der Hoek, K. Pyrc, M.F. Jebbink, W. Vermeulen-Oost, R.J. Berkhout, K.C. Wolthers, P.M. Wertheim-van Dillen, J. Kaandorp, J. Spaargaren, B. Berkhout, Nat. Med. 10 (2004) 368–373.
[3] P.C. Woo, S.K. Lau, C.M. Chu, K.H. Chan, H.W. Tsoi, Y. Huang, B.H. Wong, R.W. Poon, J.J. Cai, W.K. Luk, L.L. Poon, S.S. Wong, Y. Guan, J.S. Peiris, K.Y. Yuen, J. Virol. 79 (2005) 884–895.
[4] W. Li, Z. Shi, M. Yu, W. Ren, C. Smith, J.H. Epstein, H. Wang, G. Crameri, Z. Hu, H. Zhang, J. Zhang, J. McEachern, H. Field, P. Daszak, B.T. Eaton, S. Zhang, L.F. Wang, Science 310 (2005) 676–679.
[5] S.K. Lau, P.C. Woo, K.S. Li, Y. Huang, H.W. Tsoi, B.H. Wong, S.S. Wong, S.Y. Leung, K.H. Chan, K.Y. Yuen, Proc. Natl. Acad. Sci. USA 102 (2005) 14040–14045.
[6] Y.J. Tan, S.G. Lim, W. Hong, Antiviral. Res. 65 (2005) 69–78.
[7] C.Y. Chou, C.H. Chien, Y.S. Han, M.T. Prebanda, H.P. Hsieh, B. Turk, G.G. Chang, X. Chen, Biochem. Pharmacol. 75 (2008) 1601–1609.
[8] U. Bacha, J. Barrila, S.B. Gabelli, Y. Kiso, L. Mario Amzel, E. Freire, Chem. Biol. Drug Des. 72 (2008) 34–49.
[9] N. Barretto, D. Jukneliene, K. Ratia, Z. Chen, A.D. Mesecar, S.C. Baker, J. Virol. 79 (2005) 15189–15198.
[10] M.A. Clementz, Z. Chen, B.S. Banach, Y. Wang, L. Sun, K. Ratia, Y.M. Baez-Santos, J. Wang, J. Takayama, A.K. Ghosh, K. Li, A.D. Mesecar, S.C. Baker, J. Virol. 84 (2010) 4619–4629.
[11] K. Ratia, K.S. Saikatendu, B.D. Santarsiero, N. Barretto, S.C. Baker, R.C. Stevens, A.D. Mesecar, Proc. Natl. Acad. Sci. USA 103 (2006) 5717–5722.
[12] J.A. Wojdyla, I. Manolaridis, P.B. van Kasteren, M. Kikkert, E.J. Snijder, A.E. Gorbalenya, P.A. Tucker, J. Virol. 84 (2010) 10063–10073.
[13] N. Strater, L. Sun, E.R. Kantrowitz, W.N. Lipscomb, Proc. Natl. Acad. Sci. USA 96 (1999) 11151–11155.
[14] H.P. Chang, C.Y. Chou, G.G. Chang, Biophys. J. 92 (2007) 1374–1383.
[15] C.Y. Chou, Y.L. Lin, Y.C. Huang, S.Y. Sheu, T.H. Lin, H.J. Tsay, G.G. Chang, M.S. Shiao, Biophys. J. 88 (2005) 455–466.
[16] H.C. Chang, L.Y. Chen, Y.H. Lu, M.Y. Li, Y.H. Chen, C.H. Lin, G.G. Chang, Biophys. J. 93 (2007) 3977–3988.
[17] W.C. Hsu, H.C. Chang, C.Y. Chou, P.J. Tsai, P.I. Lin, G.G. Chang, J. Biol. Chem. 280 (2005) 22741–22748.
[18] Y.H. Hsieh, C.Y. Chou, J. Biomed. Sci. 18 (2011) 4.
[19] C.Y. Chou, W.P. Jen, Y.H. Hsieh, M.S. Shiao, G.G. Chang, J. Biol. Chem. 281 (2006) 13333–13344.
[20] S.C. Cheng, G.G. Chang, C.Y. Chou, Biophys. J. 98 (2010) 1327–1336.
[21] P. Schuck, Biophys. J. 78 (2000) 1606–1619.
[22] P.H. Brown, P. Schuck, Biophys. J. 90 (2006) 4651–4661.
[23] C.Y. Chou, Y.H. Hsieh, G.G. Chang, Methods 54 (2011) 76–82.
[24] C.N. Pace, Trends Biotechnol. 8 (1990) 93–98.
[25] N.A. Morjana, B.J. McKeone, H.F. Gilbert, Proc. Natl. Acad. Sci. USA 90 (1993) 2107–2111.
[26] D. Shortle, Adv. Protein Chem. 46 (1995) 217–247.
[27] A.L. Fink, Methods Mol. Biol. 40 (1995) 343–360.
[28] H.C. Hung, G.G. Chang, Biophys. J. 81 (2001) 3456–3471.

[29] J.A. Morrow, D.M. Hatters, B. Lu, P. Hochtl, K.A. Oberg, B. Rupp, K.H. Weisgraber, J. Biol. Chem. 277 (2002) 50380–50385.
[30] M. Hu, P. Li, M. Li, W. Li, T. Yao, J.W. Wu, W. Gu, R.E. Cohen, Y. Shi, Cell 111 (2002) 1041–1054.
[31] M. Hu, P. Li, L. Song, P.D. Jeffrey, T.A. Chenova, K.D. Wilkinson, R.E. Cohen, Y. Shi, EMBO J. 24 (2005) 3747–3756.
[32] M. Renatus, S.G. Parrado, A. D'Arcy, U. Eidhoff, B. Gerhartz, U. Hassiepen, B. Pierrat, R. Riedl, D. Vinzenz, S. Worpenberg, M. Kroemer, Structure 14 (2006) 1293–1302.
[33] X. Chen, C.Y. Chou, G.G. Chang, Antiviral. Chem. Chemother. 19 (2009) 151–156.
[34] W.L. DeLano, The PyMOL Manual, DeLano Scientific, San Carlos, CA, 2002.